

Second harmonic imaging of membrane potential of neurons with retinal

Boaz A. Nemet
Volodymyr Nikolenko
Rafael Yuste

Columbia University
Department of Biological Sciences
1212 Amsterdam Avenue
New York, New York 10027

Abstract. We present a method to optically measure and image the membrane potential of neurons, using the nonlinear optical phenomenon of second harmonic generation (SHG) with a photopigment retinal as the chromophore [second harmonic retinal imaging of membrane potential (SHRIMP)]. We show that all-trans retinal, when adsorbed to the plasma membrane of living cells, can report on the local electric field via its change in SHG. Using a scanning mode-locked Ti-sapphire laser, we collect simultaneous two-photon excited fluorescence (TPEF) and SHG images of retinal-stained kidney cells and cultured pyramidal neurons. Patch clamp experiments on neurons stained with retinal show an increase of 25% in SHG intensity per 100-mV depolarization. Our data are the first demonstration of optical measurements of membrane potential of mammalian neurons with SHG. SHRIMP could have wide applicability in neuroscience and, by modifying rhodopsin, could in principle be subject for developing genetically engineered voltage sensors. © 2004 Society of Photo-Optical Instrumentation Engineers. [DOI: 10.1117/1.1783353]

Keywords: neurons; second harmonic generation; imaging; retinal; membrane potential, nonlinear optical microscopy, rhodopsin, patch clamp.

Paper 034005 received Oct. 1, 2003; revised manuscript received Jan. 2, 2004; accepted for publication Jan. 9, 2004.

1 Introduction

In the central nervous system (CNS), information is relayed and processed by neurons that communicate by sending and receiving electrical signals. Each cell's transmembrane potential thus encodes information. Therefore, a first-order problem in the study of the brain's functioning is how to record this electrical activity from multiple neurons and their processes. An accurate measurement of the instantaneous voltage map could enable researches to decipher the architecture of the CNS and the basic rules of integration and computation it performs.

Although electrode measurements have contributed greatly to our understanding of neural physiology, it is clear that further progress requires parallel and noninvasive probing of voltage. An optical technique seems ideal, since it can satisfy both of these requirements. Following this reasoning, efforts in microscopy extending back several decades have concentrated on the use of fluorescence or absorption voltage-sensitive dyes.^{1–7} While this work has produced accurate measurements of membrane potential in single cells and in neuronal networks in invertebrate preparations, its applicability to mammalian CNS has been generally limited by the small signals and toxic effects that preclude single-cell resolution. As an alternative strategy, in the last decade, the groups of Lewis and Loew have pioneered the application of second harmonic generation (SHG) to living cells and also to measurements of membrane potential.^{8–15}

It was argued that with SHG, as opposed to standard fluorescence techniques, the fundamental laser beam can be infrared and the light-matter interaction depends nonlinearly on the photon flux density, so therefore scattering and out of focus photobleaching would be greatly reduced. The same argument has been used in favor of two-photon excited fluorescence (TPEF) microscopy.¹⁶ Two points that in particular motivate using SHG over fluorescence-based techniques for membrane potential measurements are as follows. 1. The SHG signal, as opposed to fluorescence or TPEF, can originate predominately from the membrane. This occurs because the chromophore molecules, which interact with the excitation light to give rise to hyper-Rayleigh scattering (HRS), orient themselves in the membrane and create a distribution lacking a center of symmetry, which is required for SHG but not for fluorescence. This makes SHG an ideal technique for optical probing of membranes and other chemical interfaces, particularly in the absence of noncentrosymmetric polymers, such as collagen fibers. In addition, the dye molecules that are oriented in the membrane, as opposed to free molecules in the cytoplasm, are ensured to probe the electric field across the membrane, since their axis of charge transfer—induced by the light field excitation—is roughly perpendicular to the membrane surface and therefore parallel to the electric field.¹⁷ 2. Although SHG is enhanced by proximity of the excitation wavelength to single or two-photon resonance, such a condition promotes undesirable fast photobleaching. Unlike TPEF, the SHG process does not require absorption of light, and at least in principle there should be an optimal wavelength of operation in which the SHG signal is strong enough (in terms of signal-to-

Address all correspondence to Boaz Nemet, Columbia University, Department of Biological Sciences, 1212 Amsterdam Avenue, New York, NY 10027, USA. Tel: 212-854-5023; Fax: 212-865-8246; E-mail: bn2010@columbia.edu

noise ratio), but at the same time absorption and therefore photobleaching is minimized. Since the strongest signal is presumably on-resonance (but also the fastest photobleaching occurs there), we expect that the right compromise is found at an off-resonance wavelength. It is also known that the best wavelength in terms of SHG voltage response is found off-resonance,¹⁸ which makes it consistent with the choice for optimal wavelength.

The strategy pursued so far has been the synthesis of organic dyes, based on amphiphilic styryl molecules with distinct electrochromic properties, originally synthesized for fluorescence voltage measurements.^{8,15,19,20} More recently, an important contribution to the theory of membrane imaging by SHG and methods involved in characterizing these dyes' nonlinearities and their response to voltage changes was made by the group of Mertz and Moreaux et al.,^{18,21–25} who have expanded on the work of Lewis and Loew.

As an alternative strategy to styryl dyes, we have explored the idea of using a naturally occurring chromophore to perform the task of reporting on the membrane voltage through SHG. Our first intuition suggested the protein bacteriorhodopsin (BR) could be a good candidate. Specifically, previous work has shown that the so-called purple membrane, which contains an ordered crystalline array of the protein BR, has remarkable nonlinear optical properties, one of which is SHG, and that the chromophoric group responsible for these properties is the retinal molecule.^{13,26–29}

It was even proposed and demonstrated by Lewis et al. that polyvinyl alcohol films of oriented BR can be used as an erasable optical storage medium, where nondestructive off-resonance readout was achieved by SH microscopy.³⁰

The study of rhodopsins and retinals has been wide in the biological, chemical, and physical disciplines, and there is extensive literature on the subject (see for example Refs. 31 and 32).

The photopigment all-trans retinal has a relatively small ground state dipole moment. However, it exhibits a large change in dipole moment ($\Delta\mu$) upon light excitation,³³ and more specifically, all-trans retinal has one of the largest $\Delta\mu$ compared to other forms of the chromophore.^{13,27,34} In the two-level model, the second-order molecular polarizability β is directly proportional to $\Delta\mu$.³⁵ In retinal, β is dominated by a single axial component β_{zzz} , where z is the long axis of the molecule.²⁸ A dense distribution of aligned retinal molecules is therefore expected to give a strong SHG signal.

These optical properties, perhaps expected from a chromophore that has been selected by evolution as the one photopigment to interact with all the rhodopsin proteins regardless of their function (visual or bacterial), appear ideally suited for SHG microscopy. In addition, retinal is lipophilic, which facilitates binding to biological membranes and has a well studied photophysics.^{31,36} All-trans retinal, also known as vitamin A aldehyde, is a metabolite of vitamin A and is commercially available and inexpensive. Retinal exists in a large variety of natural and synthetic forms³⁷ and, finally, its optical properties can in principle be subject to modification by genetic engineering of rhodopsin or BR. Therefore, although we did not need to take advantage of this possibility for our experiments with cultured cells, where bath application of retinal sufficed, it is conceivable that retinal-based genetically encoded voltage sensors could be developed, whereby target-

ing of retinal rhodopsin to particular neurons³⁸ or particular parts of a neuron could enable a specific second harmonic retinal imaging of membrane potential (SHRIMP) signal.

2 Materials and Methods

Hippocampi from newborn Sprague Dawley rats were dissociated and plated at low density on poly-L-lysine-coated 12-mm-diam round cover glasses, without glial support cells, following standard protocols^{39,40} and with minimal modifications. For serum-free growing media, we used NeuroBasal media (Gibco 21103-049, Invitrogen Corp., Carlsbad, California) with 0.5-mM L-glutamine (Sigma G-8540, Sigma-Aldrich Corp., St. Louis, Missouri) and 1×B-27 (Gibco 10889-038). Culture media was changed twice a week by substituting ~50% volume of old media with fresh ones. Culture media contained 0.8- μ M cytosine arabinoside (Sigma C6645) prior to the first media change to slow down glia cell proliferation.

Cells from 7 to 28 day-old cultures were used for experiments. Recordings from pyramidal neurons were made whole-cell patch-clamp configurations (using a BVC-700 amplifier, Dagan Corp., Minneapolis, Minnesota). Conventional patch pipettes (4 to 12 M Ω) contained 120-mM K-gluconate, 10-mM KCl, 5-mM ATP, 0.3-mM GTP, and 10-mM K-Hepes (pH 7.2). The extracellular recording solution contained: 119-mM NaCl, 2.5-mM KCl, 2-mM CaCl₂, 1-mM MgCl₂, 30-mM glucose, 25-mM Na-HEPES (pH 7.4)³⁸ with an addition of 100- μ M Trolox (Aldrich 23881-3) to help against photodamage during imaging.

For neuronal cultures, all-trans retinal aldehyde (Sigma 2500, powder) was dissolved first in dimethyl sulfoxide (DMSO, Sigma D-8779) in a high concentration of 100 mM, and staining was done in the incubator for 15 to 20 min. The retinal in DMSO was diluted 1/4000 into the growth medium to give a final concentration of 25- μ M retinal and 0.025% DMSO. The cover glass was then put into the microscope chamber containing the extracellular recording solution at room temperature. The retinal was kept under low light illumination and preferably under red light. Storage of the stock solutions in DMSO and in EtOH was kept at -20 °C in the dark after puffing argon gas to minimize oxygenation.

A 293S human embryonic kidney (HEK) cell line expressing rhodopsin at 3 · 10⁶ copies/cell and their control nonexpressing rhodopsin cells were obtained from Johns Hopkins University. They were grown in standard DMEM medium (Gibco 11320033) at 37 °C, and when confluence was high, they were split to dishes by Trypsin/EDTA. An extracellular medium in the microscope chamber phosphate buffer solution (PBS) was used.

HEK cells were stained with all-trans retinal that was dissolved first in EtOH to 100-mM concentration and then applied directly to the side of the dish containing the cells at a final concentration of 50 μ M.

The optical setup used for imaging is based on a modified confocal Fluoview microscope (Olympus America, Inc., Melville, New York) with an upright BX50WI, which is used in our laboratory routinely as a two-photon microscope. It is described in details in Ref. 41. The main additional feature that was used in some of the experiments (not with the HEK cells) is the addition of lock-in detection and amplification of

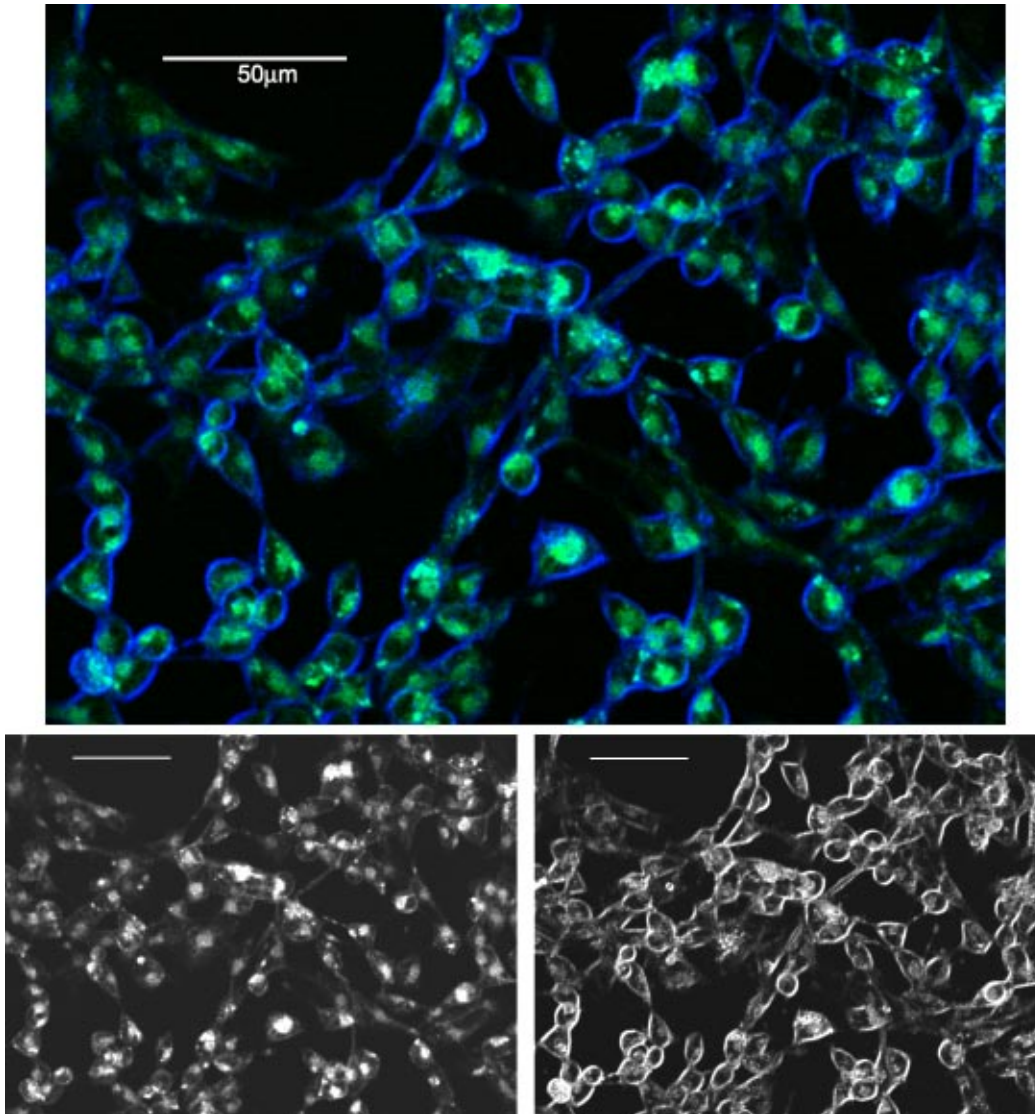


Fig. 1 Imaging retinal SHG of kidney cells. Composite image of SHG (blue) and TPEF (green) HEK 293 cells (not expressing rhodopsin) stained with all-trans retinal $50 \mu\text{M}$ in extracellular solution, laser power $\sim 20 \text{ mW}$ at 850 nm , circularly polarized light, and $30\text{-}\mu\text{s}$ pixel dwell time. $20\times$ magnification objective lens NA 0.5 was used with the normal condenser lens NA 0.8. Below the individual SHG (right) and TPEF (left) images are shown. The TPEF image is enhanced using a look-up table adjustment.

the SHG signal. The laser used was an ultrafast Ti-sapphire laser [Coherent Inc. (Santa Clara, California) MIRA basic with 150-fs pulse width and 76-MHz repetition rate, tunable range of 700 to 930 nm] and in some cases Nd:glass (High-Q Laser IC-100 with fixed 1060-nm wavelength, 100-fs pulse width, and 65-MHz repetition rate). The laser output was modulated at frequencies in the range 100 to 800 kHz by the Pockel's cell (Quantum Technology model 327, schematic is shown in Ref. 41) and a function generator (Tektronix CFG253) connected to the electro-optic (EO) modulator driver. The output of the photomultiplier tube (PMT) (Hamamatsu HC125-02), which was placed in the transmission path (after a 0.8-NA condenser by Olympus) was amplified by an analog preamplifier (Signal Recovery model 5113), and then input to the digital lock-in amplifier (Signal Recovery 7280 DSP). An analog output from the lock-in amplifier was fed to the Olympus Fluoview data acquisition box. In front of the PMT a small bandpass interference filter (Chroma Technology Corporation) 20 or 40 nm wide centered at half the excitation wavelength was placed to block the fundamental laser light and any fluorescence light.

We confirmed that the signal from retinal was a result of SHG by imaging a group of neurons using a monochromator (Bauch and Lomb Incorporated, 1350 grooves/mm cat 33-86-02) at different wavelength settings. The monochromator was placed temporarily, instead of the usual bandpass and IR blocking filters, in front of the PMT and an additional lens was used to collect the light to the entrance slit. The signal was weak but detectable. We then fitted the resulting average frame values at the different wavelengths to a Lorentzian function. The bandwidth obtained was ~ 7 nm centered exactly at half the center wavelength of the excitation light. This was evidence that the photons detected by the PMT were indeed SHG and not fluorescence photons.

3 Results and Discussion

3.1 Imaging Retinal SHG from Kidney Cells and Cultured Neurons

Our first trials were carried out on a strain of human embryonic kidney cells (HEK 293), which expresses the mammalian rhodopsin protein in their membranes. In the course of these experiments, it was discovered that the reconstitution of external all-trans retinal was necessary for the production of SHG, and moreover, there was no apparent difference between the rhodopsin expressing cells and the control cells, in terms of the SHG signal. Both strains have shown very strong SHG signals after the addition of all-trans retinal (ATR) into the extracellular medium (see next). We therefore concluded that all-trans retinal by itself is sufficient to produce SHG in these cells and presumably in other types of cells. The retinal molecules bind to the outer leaflet of the cell membrane by lipophilic attraction and orient themselves even in the absence of rhodopsin.

In Fig. 1 we show simultaneous images of SHG and TPEF of HEK 293 cells and a composite image of the two. Cells were grown on cover glass in culture prepared from a cell line that does not express rhodopsin. Similar images were acquired of the rhodopsin expressing cells, in which the signal strength was comparable (not shown). The main feature is that SHG originates predominantly from the membrane, although

some retinal was internalized, as can be seen from the fluorescence signal from within the cells, presumably accumulated in internal membranes of the endoplasmic reticulum (ER) and Golgi apparatus. The multiphoton excited fluorescence—although very weak compared with the SHG (for presentation purposes the TPEF channel is enhanced in the image)—was detectable only after incubation with 50- μ M retinal for a period of roughly 20 min. Therefore, the endogenous autofluorescence cannot account for this signal. What is striking is that the SHG signal from the membrane is accompanied only by a very weak fluorescence compared to the cytoplasmic TPEF. The reasons for that are still not clear at this point. The image in Fig. 1 was taken shortly after modifying our two-photon scanning microscope for the purpose of SHG microscopy,⁴¹ and it does not include the lock-in amplifier, later added to the setup. This explains the relatively high average power (~ 20 mW at the sample) that was needed to produce an image with such clarity.

Figure 2 shows an example of SHG imaging of rat hippocampus pyramidal neurons stained with ATR. It shows a high spatial resolution both in the plane of the image and in the axial (z) direction. The latter is a result of the nonlinear optical nature of the SHG process. Even though the neurons are grown on a cover glass and their morphology is essentially planar, unlike the situation in the real brain, the cell's somata are seen at the first image and the dendrites are clearly visible at the second image, which is focused 2- μ m closer to the cover glass. Here we used lock-in detection to amplify the SHG signal. High-frequency modulation of 800 kHz using an EO modulator and a short time constant of 10 μ s allow noise rejection and high gain while maintaining relatively high data rates. The scanning pixel dwell time was 30 μ s, which allows three time constants per pixel. In the raw data of the two images of Fig. 2, the full (12-bit) dynamic range is used and the signal at the soma is even saturated at some points, whereas the background is essentially zero. Note that the laser was polarized in the direction of the y axis of the image and therefore the horizontal membranes of the dendrites and soma appear to have a stronger signal. This is in agreement with the assumption that the retinal molecules are oriented roughly perpendicular to the membrane surface.

3.2 SHRIMP Signal Reflects Membrane Voltage

To measure the changes in SHG signal as a function of membrane potential, we used the patch clamp technique. In this procedure, a thin glass electrode filled with the right salt solution is introduced into the cell's cytoplasm, and a giga-ohm seal is formed by the membrane around it. A pyramidal neuron from rat hippocampus, which was grown in dissociated culture on a glass substrate, was patched and stimulated to fire action potentials. After verifying that the cell was healthy and excitable by electrically recording action potentials in current clamp, we switched to voltage clamp, where the cell membrane was held at -70 mV with respect to the ground electrode in the extracellular medium. An image of the patched neuron is shown in Fig. 3(a). The laser was then scanned over the cell at the same line (shown in green) repeatedly, and an $x-t$ image was recorded of the SHG signal while the voltage was switched 89 times between 0 and -70 mV every 40 scan lines (200-ms interval). In Fig. 3(b), we show the temporal

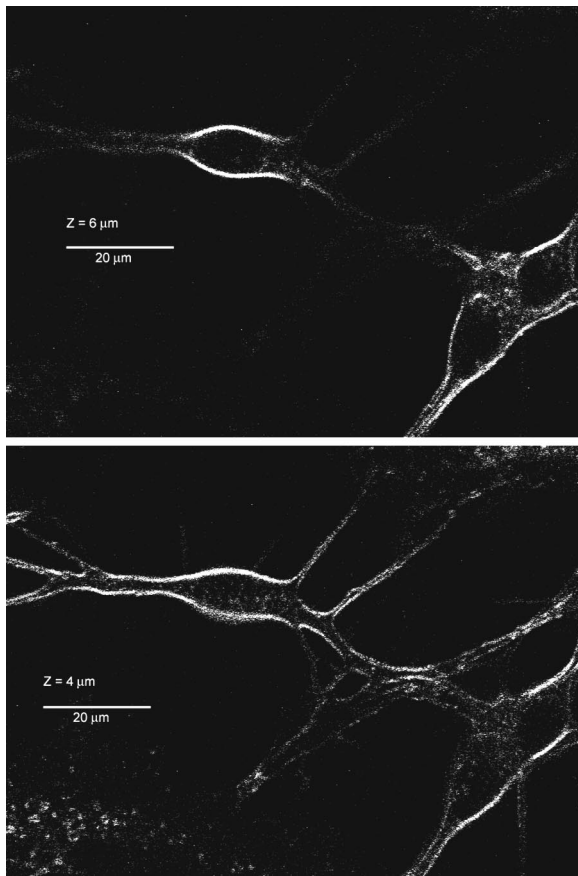


Fig. 2 Imaging retinal SHG of neurons. SHG images of rat hippocampus pyramidal neurons in dissociated culture, stained with 25- μM all-trans retinal. The two images are separated by 2 μm in the z axis (where z is the vertical distance from the cover glass surface). An Olympus objective lens of 60 \times magnification NA 0.9, and condenser lens NA 0.8 were used. Laser average power at the sample ~ 4 mW at 900 nm, linearly polarized light (in the y axis of the image), 30- μs pixel dwell time, lock-in amplifier used with 800-kHz modulation frequency, and time constant of 10 μs . No Kalman frame averaging and no image processing was done on the images except for some enhancement of the lower pixel values by limiting the maximum value in the look-up table to 1332 (from the original 4095).

mean of the line scan where the two graphs correspond to the two voltages. The two peaks correspond to the points where the laser beam crosses over the left and right membrane (vertical) walls of the neuron, where the curvature of the membrane yields a strong signal. The difference between the signals at the two voltages at the peaks are 18.4 and 18.9% for the right and left membranes, respectively (calculated for five points around the peaks). The significance of these values was tested both in the time and spatial domains. First, two time series corresponding to the two voltages were generated from the value at the membrane (average of three pixels centered at the peak of the x profile) at every time point. We then performed a standard t test for two independent populations, which resulted in the different values for the means and a significance parameter $p = 1.66 \cdot 10^{-4}$, $N = 3560$. The second significance test was done by taking the two x profiles (for the two voltages) shown in Fig. 3(b) and performing a t test for two paired populations (the values depend on the x position of

each pair) on five points centered at the peak. The result of this test was again two significantly different populations with $p = 4 \cdot 10^{-3}$, $N = 5$. We note that taking more than five points around the peak actually results in a smaller p value (more significant difference), but the difference between the two mean values for the two populations is slightly reduced and can lead to underestimation. This can be easily understood when one considers that away from the membrane, the signal approaches zero and so does the difference. A similar test was done on the left membrane data with similar results.

We repeated this procedure for a voltage step of 40 mV (-70 and -30 mV) and 20 mV (-70 and -50 mV), the results from these voltage clamp experiments are summarized in Fig. 3(c), where we plotted the percentage change in SHG for the left- and right-hand membranes. The result of the linear regression gives a slope of $25.4\% \pm 0.7\%$ increase in SH signal for 100-mV depolarization of the cell's membrane with correlation coefficient $R = 0.9949$ and $p < 0.0001$ significance parameter. Due to photobleaching and to deterioration in the health of the cell during scanning, the experiments with the voltage step of 40 and 20 mV (which were done after the 70-mV step scan) yielded a less significant result using the t tests than the first experiment. We nonetheless include these results, since they are consistent with the expected linear dependency of SHG on voltage.

3.3 SHRIMP Toxicity and Phototoxicity

All-trans retinal is a hydrophobic molecule and therefore requires the addition of a nonpolar solvent, which is undesirable but necessary in many other labeling procedures of different fluorescent markers. Although other groups seem to be able to image neurons stained with retinal using ethanol,³⁸ our neurons seem to be healthier with the DMSO as the solvent rather than the ethanol. In our hands, the DMSO became toxic for hippocampal cultured neurons at concentrations greater than 0.05%. The retinal/DMSO when added to the cell culture seemed to become toxic when incubated for more than 20 min without wash. The toxicity was evaluated by observing the integrity of the cells' membrane under a conventional light microscope. However, the cells were well stained and healthy if this time limit was kept during labeling. Rather than toxicity due to the solvent, the greatest challenge in these types of experiments was to perform patch clamp recording on the previously labeled neurons, since we found it difficult to obtain a good electric seal (~ 1 G Ω is needed) between the patch pipette and the cell membrane after staining, presumably due to the deposition of retinal and DMSO molecules on the cellular membranes, which create a kind of screening of membrane by adsorbing to the glass of the pipette.

Photodamage was observed in some cases when the laser average power was increased beyond 10 mW at the sample (and using a 0.9-NA objective lens) and the laser was pointed to a particular point at the membrane for duration of more than 100 ms for ~ 50 times intermittently. In these cases a visible change—strong bleaching and a distortion of the membrane nearby—could be seen in the neuron's membrane at the point, judging by the SHG image. We did not observe dramatic changes in cell health when the laser light was kept under 10 mW at the sample, and regular scanning was used. To illustrate this point, the cells in Fig. 2 look perfectly

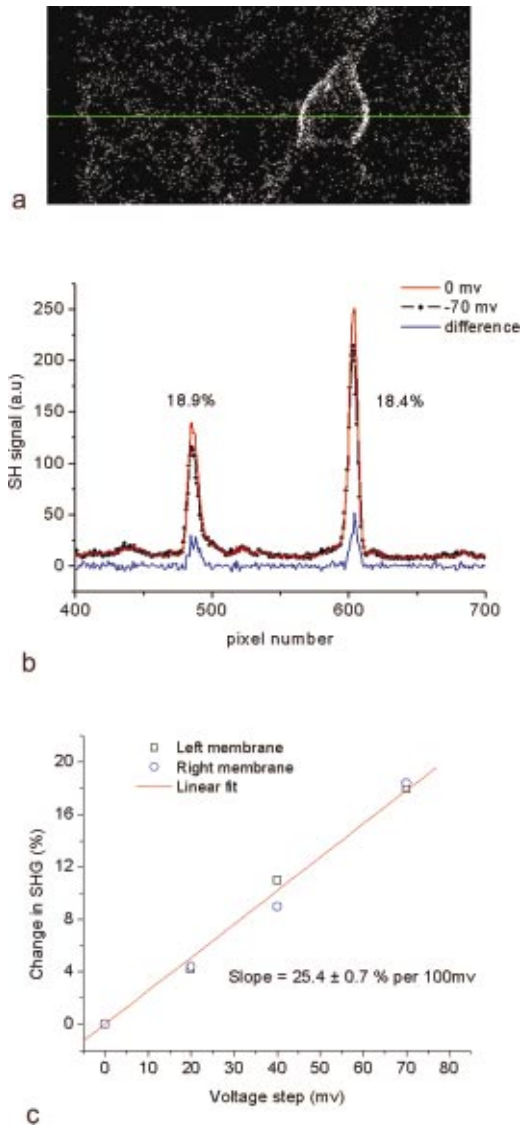


Fig. 3 Retinal SHG is sensitive to membrane voltage. (a) SHG image of rat hippocampus pyramidal neuron under patch clamp. The green line is the chosen *x**t* line scan going through the soma membrane. Fastest scan speed of 2 μ s per pixel was used without lock-in detection, and laser power 5 mW at the sample at 880 nm. (b) *x* profile averaged over time for the two voltages. The difference profile is also shown in blue. The difference in percentage is also shown at the two peaks (the left and right membrane walls). (c) Percentage change in SHG signal as a function of voltage step. The slope obtained from linear regression through the origin with correlation coefficient $R=0.99498$ and $p<0.0001$ significance parameter.

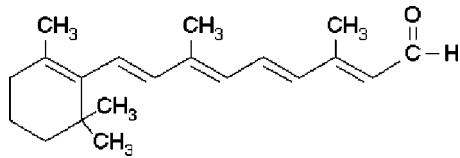


Fig. 4 Chemical structure of all-trans retinal aldehyde.

healthy, as can be seen by the integrity of their membrane and their processes. Unhealthy neurons develop beaded dendrites.

3.4 Reverse Polarity of the SHRIMP Signal

We found it surprising that for retinal the SHG signal actually increases with depolarization of the membrane, whereas in all other studies that use other molecules for SHG measurements of membrane potential, the signal decreases with depolarization. To explain the differences in behavior, one has to consider the permanent molecular dipole of the dye and its direction in the membrane as well as the induced dipole moment change. It is usually assumed in the two-level model that the excited state possesses a larger dipole moment than the ground state.¹⁵ It is known that upon light excitation of ATR, there is a net negative charge moving away from the β -ionone ring toward the aldehyde group^{33,42} (see Fig. 4 for molecular structure of ATR). Langmuir-Blodgett trough experiments²⁷ suggest that the molecular alignment of ATR in the membrane is such that the aldehyde group faces the water interface and the ionone ring is inside the lipid bilayer. It is also known that both the permanent dipole (μ_g) and the induced change in the dipole ($\Delta\mu$) point toward the ionone ring.^{33,34} We can conclude therefore that the small permanent dipole of ATR is directed toward the cytoplasmic side and is in the same direction as the electric field in the membrane at resting conditions in which the cell is more negative than the extracellular environment. This is in contrast to the amphiphilic styryl dyes such as di-4-ANEPPS,⁹ which have the opposite polarity in the membrane. We therefore propose that the reverse polarity of the dipole moment and subsequently $\Delta\mu$ may explain at least qualitatively why the response to voltage change has the opposite effect on SHG intensity.

It seems reasonable to assume that the mechanism for the SHG response to voltage changes in the membrane-bound retinal is mainly of electro-optic origin through the induced dipole moment change,^{15,18} but we cannot rule out additional realignment contributions.²² However, the increase in SHG with decreasing electric field strength suggests that reorientation is not the main contributor to the response and may even be a weakening factor in the response.

3.5 SHRIMP Bleaching and Wavelength Dependency

As discussed in the introduction, SHG can be obtained off-resonance and therefore SHG imaging can be made with significantly reduced photobleaching, which can in some cases create a serious problem. For example, to optically detect fast biological events like action potentials that take place on the time scale of milliseconds, one cannot use the laser beam to scan a wide area. There is a tradeoff between field of view and temporal resolution. In the extreme case when the laser beam is parked at one position on the membrane and the laser shutter is opened, we notice very fast photobleaching of the SH

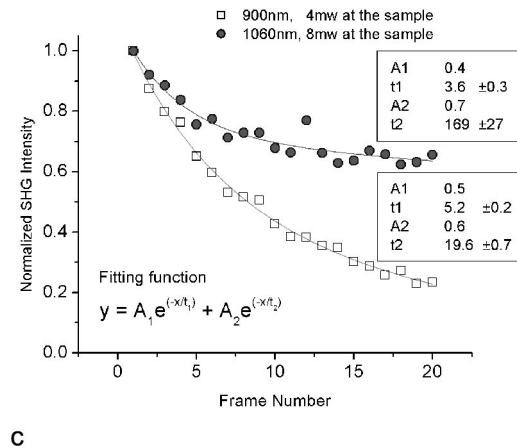
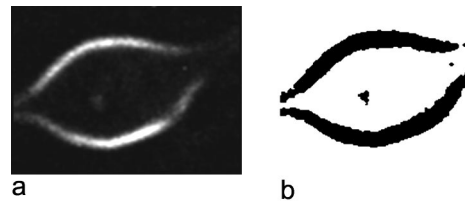


Fig. 5 Photobleaching of retinal SHG. (a) Time averaged (20 frames) SHG image of a neuron stained with ATR. Laser used was an ultrafast Nd:glass laser from High-Q Lasers, operating at 1060 nm. Pixel clock of 10 μ s (2 s per frame). (b) Threshold image showing the selected membrane pixels, which are used for averaging. (c) Photobleaching curves for two excitation wavelengths 900 nm (Ti-sapphire laser) and 1060 nm (Nd:glass laser). 20 frames were taken sequentially as an *xyt* movie. Each point in the graph represents the average pixel value of that frame calculated for the membrane pixels [shown in Fig. 4(b)].

signal at a rate of tens of milliseconds with moderate laser power of less than 10 mW at 850 nm (data not shown). We also noticed partial recovery if one allows for some time to pass between openings of the shutter, possibly from 2-D diffusion along the membrane. The process of SHG bleaching in the membrane is not well understood, although some models exist. One such model supports a light-induced flip-flop mechanism²³ of the amphiphilic dye molecules going from one leaflet of the membrane to the other, and thus spoiling the asymmetrical distribution and reducing SHG. The bleaching could also be due to light-induced conformational change from all-trans to cis configuration, which has a smaller $\Delta\mu$, or simply a result of bond breaking and loss of HRS from these molecules. Since surface SHG depends quadratically on the number density of molecules that generate HRS,^{21,25} SHG bleaching would occur even at a faster rate than bleaching TPEF, which depends linearly on the number of fluorescent molecules.

We wanted to explore the possibility of reducing SHG photobleaching by operating at a wavelength away from resonance and preferably at a longer wavelength. Since ATR has a single photon resonance around 380 nm, we decided to test the bleaching rate at 900 nm with the Ti-sapphire laser and at 1060 nm with the Nd:glass laser. Indeed, the results shown in Fig. 5 convince us that at this range, longer wavelength reduces photobleaching.

Figure 5(a) shows the resultant time-average (20 frames) SHG image of a neuron stained with ATR. In Fig. 5(c) we see

the photobleaching curves for two excitation wavelengths: 900 and 1060 nm. 20 frames were taken sequentially as an *xyt* movie (2 s per frame). The filters in front of the PMT were changed accordingly to 450- and 530-nm center wavelengths with a 20-nm band. Each point in the graph represents the average pixel value for one frame calculated at the membrane pixels [shown in Fig. 5(b) after applying a threshold to exclude background pixels]. It is clear from the graph that the bleaching rate is faster for the shorter wavelength. The double exponential fit reveals that there are at least two characteristic decay time scales: a fast and a slow decay. Interestingly, the 1060-nm data shows an initial fast decay $t_1 = 3.5$ frames (even faster than the 900-nm data, though with a small amplitude) and then a very slow decay $t_2 = 169$ frames. The transmission of our system (including the 60 \times IR2 Olympus objective lens) was measured in this wavelength range, and the laser power marked in the figure is after this correction has been made. Although the average power at 1060 nm in our experiments is two times greater, and pulse width is actually shorter (100 fs) than at 900 nm (150 fs for the MIRA laser), which means higher peak intensities, and accepting that the other parameters are quite similar (repetition rate, objective back aperture filling, and beam quality), photobleaching is less severe at this longer wavelength, image quality is not degraded, and longer experiments duration involving intensive imaging can be performed.

3.6 SHG versus TPEF

Optical techniques have had a great impact on neuroscience in the past and improvements in microscopy methods are changing our view of the CNS. Studying electrical signals in neurons using light only can take this field into a whole new level of sophistication and understanding. The quest for optical recording from neurons has therefore been ongoing for the last three decades and is nicely illustrated in some of the publications of Webb, who also pioneered the use of multiphoton microscopy in biological research⁴² and who recently also contributed to SHG microscopy,^{43–45} and to whom this issue of the Journal of Biomedical Optics is a tribute. We present a technique that relies on SHG, which like TPEF is a nonlinear optical phenomenon that requires very large photon fluxes. SHG has obvious advantages for membrane imaging. It is an exquisitely sensitive technique to measure interfaces^{46,47} and thus appears ideal for biological samples. We do not expect it, however, to replace TPEF, since it does not have the sensitivities that fluorescence dyes possess for chemical environments. In addition, fluorescence-based techniques have the obvious advantage of imaging green fluorescent protein (GFP) and its variants. Rather, the two techniques seem to complement each other in their functionalities and are easily realized in a laser scanning microscope, as is shown in this work and in numerous previous studies. Many of the recent applications of SHG microscopy make use of an intrinsic signal from arrangements of certain proteins such as collagen that possess the required symmetry for SHG, thus revealing specific tissue structure.^{11,44,45} Moreover, given that rhodopsin is a HRS protein that can produce SHG, we propose the possibility of imaging the retina using SHG. Although the geometry has to be changed to image the live eye, contrast images could reveal with high resolution the density distribution of rhodopsin pro-

teins and of oriented aggregates of retinal in the retina, and this could possibly lead to medical applications in diagnosing defects in the retina, as well as to the study of photochemical and photobiological mechanisms of vision.

4 Conclusions

We develop an imaging technique SHRIMP based on all-trans retinal chromophore that is capable of producing high-resolution images of live neurons, specifically neuronal membranes. We also show, by patch clamp measurements, that SHRIMP produces a voltage map of the local trans-membrane potential. Experiments on rat hippocampal neurons in a primary dissociated cell culture yield a sensitivity of 25% change in SHG intensity per 100-mV change, which is similar to the sensitivity measured in giant unilamellar vesicles and cultured neuroblastoma cells with synthetic styryl dyes^{8,18} but with opposite polarity. Our experiments are the first to show SHG voltage sensitivity in mammalian neurons using patch clamp recordings. Images of voltage distribution can now be obtained by SHRIMP in culture cells, and we are working to extend this to high-resolution images in acute brain slices.

Acknowledgments

We would like to thank Ken Eisenthal for useful discussions, Jeremy Nathans for the rhodopsin expressing HEK cells, Tony Heinz for the use of the monochromator, Boris Zemelman and Sonja Krane for advice on retinal, and members of the Yuste Laboratory for help and useful advice during different stages of the work. Finally, we thank Professor Webb for his support and encouragement over the years.

References

1. P. R. Dragsten and W. W. Webb, "Mechanism of the membrane potential sensitivity of the fluorescent membrane probe merocyanine 540," *Biochemistry* **17**(24), 5228–5240 (1978).
2. D. Gross, L. Loew, and W. Webb, "Optical imaging of cell membrane potential changes induced by applied electric fields," *Biophys. J.* **50**(2), 339–348 (1986).
3. D. Gross and L. M. Loew, "Fluorescent indicators of membrane potential: microspectrofluorometry and imaging," *Methods Cell Biol.* **30**, 193–218 (1989).
4. A. Grinvald, W. N. Ross, and I. Farber, "Simultaneous optical measurements of electrical activity from multiple sites on processes of cultured neurons," *Proc. Natl. Acad. Sci. U.S.A.* **78**(5), 3245–3249 (1981).
5. A. Grinvald, R. D. Frostig, E. Lieke, and R. Hildesheim, "Optical imaging of neuronal activity," *Physiol. Rev.* **68**, 1285–1365 (1988).
6. W. N. Ross, L. B. Salzberg, L. B. Cohen, A. Grinvald, H. V. Davila, A. S. Waggoner, and C. H. Wang, "Changes in absorption, fluorescence, dichroism, and birefringence in stained giant axons: optical measurements of membrane potential," *J. Membr. Biol.* **33**, 141–183 (1977).
7. L. Cohen, "Optical approaches to neuronal function," in *Annual Review of Physiology*, J. F. Hoffman and P. De Weer, Eds., pp. 487–582, Annual Review Inc., Palo Alto, CA (1989).
8. A. C. Millard, P. Campagnola, W. A. Mohler, A. Lewis, and L. Loew, "Second harmonic imaging microscopy," *Methods Enzymol.* **361**, 47–69 (2003).
9. P. J. Campagnola, M. D. Wei, A. Lewis, and L. M. Loew, "High-resolution nonlinear optical imaging of live cells by second harmonic generation," *Biophys. J.* **77**(6), 3341–3349 (1999).
10. A. C. Millard, L. Jin, A. Lewis, and L. M. Loew, "Direct measurement of the voltage sensitivity of second-harmonic generation from a membrane dye in patch clamp cells" *Opt. Lett.* **28**(14), 1221–1223 (2003).
11. P. J. Campagnola, A. C. Millard, M. Terasaki, P. E. Hoppe, C. J. Malone, and W. A. Mohler, "Three-dimensional high-resolution

- second-harmonic generation imaging of endogenous structural proteins in biological tissues," *Biophys. J.* **82**(1), 493–508 (2002).
12. P. J. Campagnola, H. A. Clark, W. A. Mohler, A. Lewis, and L. M. Loew, "Second-harmonic imaging microscopy of living cells," *J. Biomed. Opt.* **6**, 277–286 (2001).
 13. A. Lewis, A. Khatchatourians, M. Treinin, Z. Chen, G. Peleg, N. Friedman, O. Bouevitch, Z. Rothman, L. Loew, and M. Sheves, "Second harmonic generation of biological interfaces: Probing the membrane protein bacteriorhodopsin and imaging membrane potential around GFP molecules at specific sites in neuronal cells of *C. elegans*," *Chem. Phys.* **245**, 133–144 (1999).
 14. G. Peleg, A. Lewis, M. Linial, and L. M. Loew, "Nonlinear optical measurement of membrane potential around single molecules at selected cellular sites," *Proc. Natl. Acad. Sci. U.S.A.* **96**(12), 6700–6704 (1999).
 15. O. Bouevitch, A. Lewis, I. Pinevsky, J. P. Wuskell, and L. M. Loew, "Probing membrane potential with nonlinear optics," *Biophys. J.* **65**(2), 672–679 (1993).
 16. W. Denk, J. H. Strickler, and W. W. Webb, "Two-photon laser scanning fluorescence microscopy," *Science* **248**(4951), 73–76 (1990).
 17. M. Bechem, S. Beutner, N. Burkhardt, C. Fuchs, C. Krysch, W. Paffhausen, B. Reiffers, A. Schade, W. R. Schlue, D. Schmid, L. Schneider, P. Schulte, T. Wimmer, D. Witzak, and H. D. Martin, "Novel hyperpolarizable and fluorescent dyes in lipid membranes: studying membrane potentials using nonlinear optical and fluorescence," *Electrochim. Acta* **48**(20–22), 3387–3393 (2003).
 18. L. Moreaux, T. Pons, V. Dambrin, M. Blanchard-Desce, and J. Mertz, "Electro-optic response of second-harmonic generation membrane potential sensors," *Opt. Lett.* **28**(8), 625–627 (2003).
 19. I. Ben-Oren, G. Peleg, A. Lewis, B. Minke, and L. Loew, "Infrared nonlinear optical measurements of membrane potential in photoreceptor cells," *Biophys. J.* **71**, 1616–1620 (1996).
 20. J. Y. Huang, A. Lewis, and L. Loew, "Nonlinear optical properties of potential sensitive styryl dyes," *Biophys. J.* **53**, 665 (1988).
 21. L. Moreaux, O. Sandre, S. Charpak, M. Blanchard-Desce, and J. Mertz, "Coherent scattering in multi-harmonic light microscopy," *Biophys. J.* **80**(3), 1568–1574 (2001).
 22. T. Pons, L. Moreaux, O. Mongin, M. Blanchard-Desce, and J. Mertz, "Mechanisms of membrane potential sensing with second-harmonic generation microscopy," *J. Biomed. Opt.* **8**(3), 428–431 (2003).
 23. T. Pons, L. Moreaux, and J. Mertz, "Photoinduced flip-flop of amphiphilic molecules in lipid bilayer membranes," *Phys. Rev. Lett.* **89**(28 Pt 1), 288104 (2002).
 24. L. Moreaux, O. Sandre, and J. Mertz, "Membrane imaging by second-harmonic generation microscopy," *J. Opt. Soc. Am. B* **17**(10), 1685–1694 (2000).
 25. L. Moreaux, O. Sandre, M. Blanchard-Desce, and J. Mertz, "Membrane imaging by simultaneous second-harmonic generation and two-photon microscopy," *Opt. Lett.* **25**(5), 320–322 (2000).
 26. J. Y. Huang and A. Lewis, "Determination of the absolute orientation of the retinylidene chromophore in purple membrane by a second-harmonic interference technique," *Biophys. J.* **55**, 835 (1989).
 27. J. Huang, A. Lewis, and T. Rasing, "Second harmonic generation from Langmuir-Blodgett films of retinal and retinal Schiff bases," *J. Phys. Chem.* **92**, 1756 (1988).
 28. Z. Chen, M. Sheves, A. Lewis, and O. Bouevitch, "A comparison of the second harmonic generation from light-adapted, dark-adapted, blue, and acid purple membrane," *Biophys. J.* **67**(3), 1155–1160 (1994).
 29. P. K. Schmidt and G. W. Rayfield, "Hyper-Rayleigh light-scattering from an aqueous suspension of purple membrane," *Appl. Opt.* **33**(19), 4286–4292 (1994).
 30. Z. Chen, A. Lewis, H. Takei, and I. Nebenzahl, "Bacteriorhodopsin oriented in polyvinyl alcohol films as an erasable optical storage medium," *Appl. Opt.* **30**, 5188 (1991).
 31. R. Birge, "Photophysics of light transduction in rhodopsin and bacteriorhodopsin," *Annu. Rev. Biophys. Bioeng.* **10**, 315–354 (1981).
 32. R. R. Birge, "Photophysics and molecular electronic applications of the rhodopsins," *Annu. Rev. Phys. Chem.* **41**, 683–733 (1990).
 33. R. Mathies and L. Stryer, "Retinal has a highly dipolar vertically excited singlet state: implications for vision," *Proc. Natl. Acad. Sci. U.S.A.* **73**(7), 2169–2173 (1976).
 34. T. Rasing, J. Hung, A. Lewis, T. Stehlin, and Y. R. Shen, "In situ determination of induced dipole moments of pure and membrane-bound retinal chromophores," *Phys. Rev. A (General Physics)* **40**, 1684 (1989).
 35. A. Oudar and O. Chemla, "Hyperpolarizabilities of the nitroanilines and their relations to the excited state dipole moment," *J. Chem. Phys.* **66**, 2664 (1977).
 36. L. Stryer, "Molecular basis of visual excitation," *Cold Spring Harb Symp. Quant Biol.* **53**, 283–294 (1988).
 37. B. Borhan, M. Souto, H. Imai, Y. Shichida, and K. Nakanishi, "Movement of retinal along the visual transduction path," *Science* **288**, 2209–2212 (2000).
 38. B. V. Zemelman, G. A. Lee, M. Ng, and G. Miesenbock, "Selective photostimulation of genetically chARGed neurons," *Neuron* **33**(1), 15–22 (2002).
 39. R. Yuste, *Imaging Neurons: A Laboratory Manual*, p. Appendix 5B, Cold Spring Harbor Press, Cold Spring Harbor, (2000).
 40. G. Banker and K. Goslin, *Culturing Nerve Cells*, pp. xiii, 453, Cellular and Molecular Neuroscience Series, MIT Press, Cambridge, MA (1991).
 41. V. Nikolenko, B. Nemet, and R. Yuste, "A two-photon and second-harmonic microscope," *Methods* **30**(1), 3–15 (2003).
 42. R. M. Williams, W. R. Zipfel, and W. W. Webb, "Multiphoton microscopy in biological research," *Curr. Opin. Chem. Biol.* **5**(5), 603–608 (2001).
 43. D. A. Dombeck, M. Blanchard-Desce, and W. W. Webb, "Optical recording of action potentials with second-harmonic generation microscopy," *J. Neurosci.* **24**(4), 999–1003 (2004).
 44. D. A. Dombeck, K. A. Kasischke, H. D. Vishwasrao, M. Ingelsson, B. T. Hyman, and W. W. Webb, "Uniform polarity microtubule assemblies imaged in native brain tissue by second-harmonic generation microscopy," *Proc. Natl. Acad. Sci. U.S.A.* **100**(12), 7081–7086 (2003).
 45. W. R. Zipfel, R. M. Williams, R. Christie, A. Y. Nikitin, B. T. Hyman, and W. W. Webb, "Live tissue intrinsic emission microscopy using multiphoton-excited native fluorescence and second harmonic generation," *Proc. Natl. Acad. Sci. U.S.A.* **100**(12), 7075–7080 (2003).
 46. Y. R. Shen, "Surface properties probed by second-harmonic and sum frequency generation," *Nature (London)* **337**, 519–525 (1989).
 47. K. B. Eisenthal, "Liquid interfaces probed by second-harmonic and sum-frequency spectroscopy," *Chem. Rev. (Washington, D.C.)* **96**(4), 1343–1360 (1996).